J Solid State Electrochem (2012) 16:1305–1312
DOI 10.1007/s10008-011-1552-z

REVIEW

Photoelectrochemical performance of bilayered $Fe–TiO_2/Zn–Fe_2O_3$ thin films for solar generation of hydrogen

Poonam Sharma · Praveen Kumar · Anjana Solanki · Rohit Shrivastav · Sahab Dass · Vibha R. Satsangi

Received: 11 April 2011 / Revised: 10 August 2011 / Accepted: 9 September 2011 / Published online: 4 October 2011

Abstract A visible-light sensitive bilayered photoanode of $Fe–TiO_2/Zn–Fe_2O_3$ has been developed by spray pyrolytically depositing $Zn–Fe_2O_3$ layers onto predeposited $Fe–TiO_2$ thin film on ITO substrate. $Fe–TiO_2/Zn–Fe_2O_3$ photoelectrodes were characterized by XRD, Raman, AFM, UV-vis absorption spectroscopy. Photoelectrochemical properties of bilayered $Fe–TiO_2/Zn–Fe_2O_3$ photoelectrode were studied by Mott–Schottky curves and I–V characteristics. Bilayered $Fe–TiO_2/Zn–Fe_2O_3$ photoelectrode was observed to possess much higher separation efficiency of photogenerated charge carriers and could generate nine times better photocurrent density than pure $Fe–TiO_2$. Solar to hydrogen conversion efficiency exhibited by this electrode was 0.77%.

Keywords Photoelectrochemical · Titanium dioxide · Iron oxide · Hydrogen

Introduction

Solar hydrogen generation from photoelectrochemical water-splitting reactions has received much attention, because of its potential as a clean source of energy in contrast to the problems raised by the use of fossil fuels [1]. The main challenge in this area is to find a suitable semiconductor exhibiting efficient splitting of water in photoelectrochemical introduce (PEC) cell. Titanium dioxide (TiO_2) is known to be an attractive material for its use as photoelectrode in PEC cells, owing to the remarkable charge-transport property, superior oxidation ability, easy access, low price, chemical stability and favourable band-edge position [2]. However, the low solar-to-hydrogen (STH) conversion efficiency is still a major barrier restricting the practical application of TiO_2 thin films. The modifications on TiO_2 semiconductor, such as doping with other elements, coupling with other semiconductors are potentially effective approaches to resolve this problem. The doping of metal or nonmetal elements, such as Fe [3, 4], S [5] or N [6] are commonly used to improve the photocatalytic activity of TiO_2 thin film. The photocatalytic activity of TiO_2 thin film has also been improved by coupling with the semiconductors such as Fe_2O_3 [7], CdS [8], ZrO_2 [9] and WO_3, etc. [10]. A proficient way is the use of low bandgap nano-semiconductors in conjunction with TiO_2 in the composite form such as in $Fe_2O_3–TiO_2$, where low bandgap Fe_2O_3 permits the solar energy absorption in visible range. As poor visible-light absorption of TiO_2 and rapid recombination property of Fe_2O_3 limits its application as photoelectrode in PEC cell. Thus, developing this type of composite structure, rather than single bandgap semiconductor devices, provides efficient charge carrier separation and more efficient matching of the solar spectra [7–11]. Recent report on TiO_2 sensitized with Fe_2O_3 has shown better photocatalytic ability as compared to single TiO_2 under visible light [12]. To check the visible light photoresponse of TiO_2 thin film sensitized with small bandgap Fe_2O_3, we designed bilayered thin films of TiO_2/Fe_2O_3, but no observable photoresponse was obtained. Since performance of Fe-doped TiO_2 ($Fe–TiO_2$) and Zn-doped Fe_2O_3 ($Zn–Fe_2O_3$) [3, 13], as single material photoelectrode, in PEC cell have been reported to be better

P. Sharma · P. Kumar · V. R. Satsangi (✉)
Department of Physics and Computer Science, Faculty of Science,
Dayalbagh Educational Institute,
Dayalbagh, Agra 282005, India
e-mail: vibhasatsangi@gmail.com

A. Solanki · R. Shrivastav · S. Dass
Department of Chemistry, Faculty of Science,
Dayalbagh Educational Institute,
Dayalbagh, Agra 282005, India

than their undoped counterpart. Therefore, in present study, we designed Fe–TiO_2/Zn–Fe_2O_3 bilayered photoelectrode capable of efficiently support the carrier transfer across the interface upon illumination under external bias. This is important to mention here that the work on double-doped Fe–TiO_2/Zn–Fe_2O_3 was started after we performed pilot experiments on TiO_2/Zn–Fe_2O_3, Fe–TiO_2/Fe_2O_3 and Fe–TiO_2/Zn–Fe_2O_3 photoelectrodes and found double-doped films exhibiting better PEC response as compared to single-doped. Fe–TiO_2 thin films were synthesized by the sol–gel/spin coating method on the conducting glass substrate (In-SnO_2), and Zn-doped Fe_2O_3 (Zn–Fe_2O_3) was overlayered onto the predeposited Fe–TiO_2 by the simple and economical spray pyrolysis method. Significantly enhanced photoelectrochemical response of Zn–Fe_2O_3 layer deposited onto Fe–TiO_2 has been reported earlier by authors group [12], where PEC response was optimized with respect to thickness of the underlying layer of Fe–TiO_2. In the present study, attempts have been made to optimize photoelectrochemical response of bilayered photoelectrode Fe–TiO_2/Zn-Fe_2O_3, with respect to thickness of the overlying Zn–Fe_2O_3 layer. We also proposed an energy band diagram for Fe–TiO_2/Zn–Fe_2O_3 to explain the charge transfer across the interface.

Experimental

Preparation of photoelectrodes

Preparation of Fe–TiO_2 thin film

Nanostructured iron-doped TiO_2 (Fe–TiO_2) thin films were deposited onto conducting glass substrate (In–SnO_2 of area 1.5×1.5 cm^2) by the sol–gel, spin coating method, the gel was obtained by mixing 20 ml of ethanol to 3 ml of titanium tetraisopropoxide, $Fe(NO_3)_3.9H_2O$ (0.2 at.% as dopant) (99.9%, Sigma Aldrich), and 1 ml of diethanolamine solution. Stirring the solution for 4 h at room temperature on a magnetic stirrer resulted in a transparent colloidal gel, which was spin-coated on a conducting glass substrate at 3,000 rpm. After each coating, the film was left for drying in an oven at 50 °C for 10 min. For the present experiment, this process was repeated twice to obtain two layers of approximately 640 nm of Fe–TiO_2 thin film as measured by alpha-step profilometer (Tencor Alpha Step 500). One third part of conducting glass substrate was initially covered by transparent tape to establish the electrical contact. Finally, the pure Fe–TiO_2 thin films were obtained.

Preparation of bilayered Fe–TiO_2/Zn–Fe_2O_3 thin film

Bilayered Fe–TiO_2/Zn–Fe_2O_3 thin films were obtained by over layering the Zn–Fe_2O_3 thin film onto Fe–TiO_2 using the spray pyrolysis setup (laboratory built and designed) [12]. The spray precursor comprising of 0.15 M $Fe(NO_3)_3.9H_2O$ and 5.0 at.% $Zn(NO_3)_2.6H_2O$ (dopant) in 100 ml of deionized water. Precursor solution was sprayed with air as carrier gas at a pressure of 2 kg cm^{-2} through a pneumatic nebulizer with a nozzle diameter of 0.1 mm onto (pre-deposited) Fe–TiO_2 thin films, kept on substrate heater at 350 °C temperature, with nearly covering one-third surface of the substrate left for contact formation in previous step with aluminium foil. The solution was sprayed for duration of 10 s with 3 min gap between each successive spray. To optimize the photoelectrochemical response of bilayered Fe–TiO_2/Zn–Fe_2O_3 thin films, 20, 40 and 60 s of spray periods were obtained with details as given in Table 1. Finally, all the thin films were heated at the rate of 2 °C min^{-1} to 500 °C and annealed for 2 h. Thus, obtained bilayered Fe–TiO_2/Zn–Fe_2O_3 thin films were semi-transparent reddish brown in appearance and strongly adherent to the substrate. Finally, Fe–TiO_2 and bilayered Fe–TiO_2/Zn–Fe_2O_3 thin films were converted into photoelectrodes using copper wire, silver paste and epoxy (Hysol, Singapore) for its use as photoelectrode in PEC cell.

Characterization

The crystallinity and phase of the thin films were investigated with an X-ray diffractometer (PANalytical X'Pert PRO θ-2θ Diffractometer) using Cu Kα irradiation. The morphology of the thin films was obtained using an atomic force microscope (Molecular Imaging, AZ, Pico SPM II). The optical absorption spectrum of the films was obtained using a spectrophotometer (Shimadzu, UV-2450). Photoelectrochemical study was carried out in a three electrode quartz cell in which pure Fe–TiO_2 and bilayered Fe–TiO_2/Zn–Fe_2O_3 thin films were used as working electrode, a saturated calomel electrode (SCE) as reference and platinum mesh as counter electrode. Electrolyte used in the cell was 1 M NaOH. The applied potential was varied from −1.0 to +1.0 V/SCE using a potentiostat (PAR, Versa Stat II).The photocurrents measured under visible light were obtained using a 150 W Xenon lamp (Bentham) with

Table 1 Description for all the thin film samples

S. no.	Film thickness (μm)		Acronym
	Fe–TiO_2	Zn–Fe_2O_3	
1	0.64	–	A_1
2	0.64	0.24	A_2
3	0.64	0.48	A_3
4	0.64	0.72	A_4

illumination intensity of 150 mW cm^{-2}. The intensity of the light source was measured using broadband power meter (Melles Griot, 13PEM001). A water jacket was placed before the light source in order to eliminate the heating effect. The resistivity for all the samples was calculated from the slope of current–voltage curves under dark condition. The experimental procedure also involves the measurement of the open-circuit photovoltage (V_{oc}) for all the samples to calculate solar-to-hydrogen conversion efficiency. To estimate the flat-band potential (V_{FB}) of the material, Mott–Schottky curves ($1/C^2$ versus V_{app}) were obtained under dark conditions in the same three-electrode configuration by measuring capacitance (C) at varying electrode potential (V_{app}) using an LCR meter (Agilent Technology, 4263 B). The flat-band potential of a semiconductor was obtained from the intercept of Mott–Schottky plot using the following relation [14]:

$$\frac{1}{C^2} = \left(\frac{2}{q\varepsilon_o\varepsilon N}\right)\left(V_{app} - V_{FB} - \frac{kT}{q}\right) \quad (1)$$

Where ε_o is the permittivity of the vacuum, N is the donor density, V_{app} is the applied potential, ε is the dielectric constant of the semiconductor, kT/q is the temperature dependent term. The intercept of linear plot at $C^{-2}=0$ gives the flat-band potential.

Results

Figure 1 shows the X-ray diffraction (XRD) patterns of Fe–TiO_2 thin film, and bilayered Fe–TiO_2/Zn–Fe_2O_3 thin films annealed at 500 °C for 2 h. The typical patterns of the anatase phase besides the peaks of ITO can be observed in curve 'A_1'. The peaks, located at 2θ=25.3° and 37.5° corresponds to the (101) and (004) orientation of the anatase phase of TiO_2 having tetragonal structure. The XRD pattern of bilayered films exhibited diffraction peaks at 24.1, 33.3, 40.9, 54.0 and 57.8°, which can be indexed to (012), (104), (113), (116) and (018) plane, respectively of the rhombohedral hematite phase of over layered iron oxide thin film in bilayered structure. Additional weak peaks in the XRD pattern of bilayered samples at 2θ=39.8° and 52.8° indicated the formation of some mixed oxides, $Ti_9Fe_3(Ti_7Fe_3)O_3$ and $FeTi_2O_5$. The formation of mixed phase could be explained by the fact that during annealing, Fe^{3+} ions of Zn–Fe_2O_3 present at the interface, diffused into the underlying Fe–TiO_2 layer producing a substitutional solid solution. In fact, as the radius of the two ions Fe^{3+} (0.55 Å) and Ti^{4+} (0.60 Å) are approximately the same [15], the substitution of iron in the matrix of TiO_2 is a favourable process [16]. Also the mixed oxide formation with the addition of the iron onto the titanium dioxide has been reported earlier [17]. The average particle size of Fe–TiO_2 as calculated from (101) peak of the XRD pattern using Scherrer's formula was increased from 24 nm (pure Fe–TiO_2) to 35 nm for bilayered samples [15].

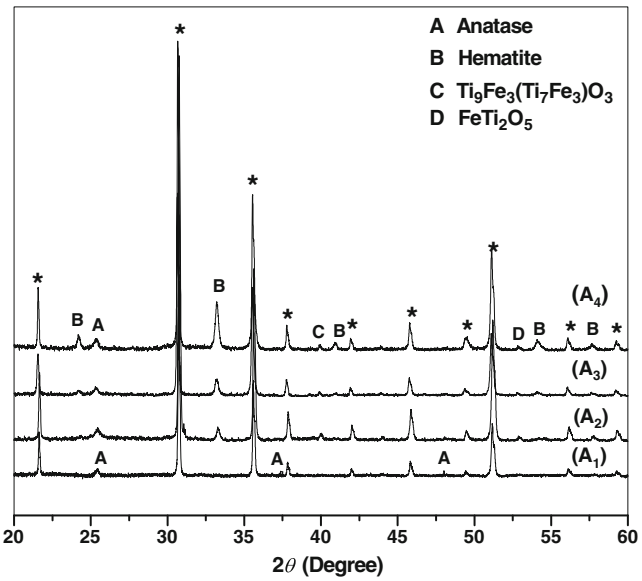

Fig. 1 X-ray diffraction pattern for pure Fe–TiO_2 and bilayered Fe–TiO_2/Zn–Fe_2O_3 thin film deposited on conducting glass substrate, ITO (In/SnO_2). *Asterisks* indicate the peaks corresponding to underlying ITO conducting glass substrate

Atomic force microscopy (AFM) images obtained for pure Fe–TiO_2 and bilayered Fe–TiO_2/Zn–Fe_2O_3 thin films have been shown in Fig. 2 along with the particle size distribution. Fe–TiO_2 thin film as deposited on ITO substrate (Fig. 2a) showed the uniform and granular surface with average particle size of 22 nm. Surface morphology of bilayered sample, having 480 nm thick upper layer of Zn–Fe_2O_3 (Fig. 2b), depicts the uniform deposition of Zn–Fe_2O_3 over Fe–TiO_2 with slightly larger grain size and porous surface morphology.

Figure 3 shows the UV-vis optical absorption spectra of Fe–TiO_2 and bilayered Fe–TiO_2/Zn–Fe_2O_3 thin films designed with varying thickness of upper layer of Zn–Fe_2O_3. Fe–TiO_2 thin film exhibited absorption in UV region with absorption edge at wavelength ~358 nm, because of its wide bandgap (Fig. 3, curve A_1). However, bilayered Fe–TiO_2/Zn–Fe_2O_3 films could absorb lower energy photons up to 593 nm as the thickness of the overlying Zn–Fe_2O_3 film increased from 240 to 720 nm, indicating that the absorption bandgap was narrowed by introduction of the Zn–Fe_2O_3 layer onto the Fe–TiO_2. It may be attributed to the formation of mixed oxides of iron and titanium of comparatively reduced optical bandgap energy around 2.0 eV. Earlier reports on the optical absorption spectra of the mixed metal oxide systems indicate that increasing iron oxide concentration in the titanium dioxide thin films leads to formation of iron–titanium mixed oxides with reduced bandgap energy nearly close to the iron oxide bandgap [18]. The optical

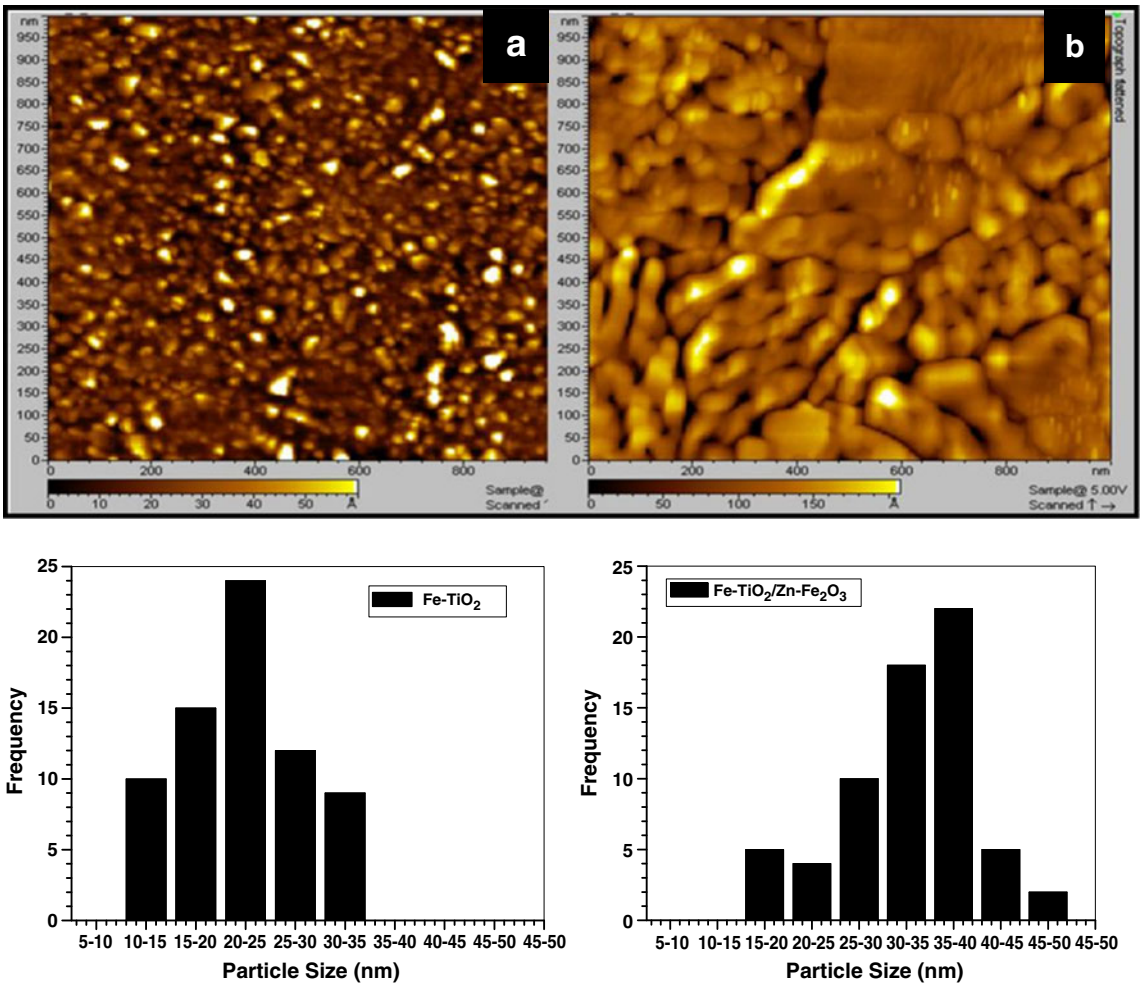

Fig. 2 AFM image with particle size distribution for (**a**) pure Fe–TiO_2 and (**b**) bilayered Fe–TiO_2/Zn–Fe_2O_3 thin film samples

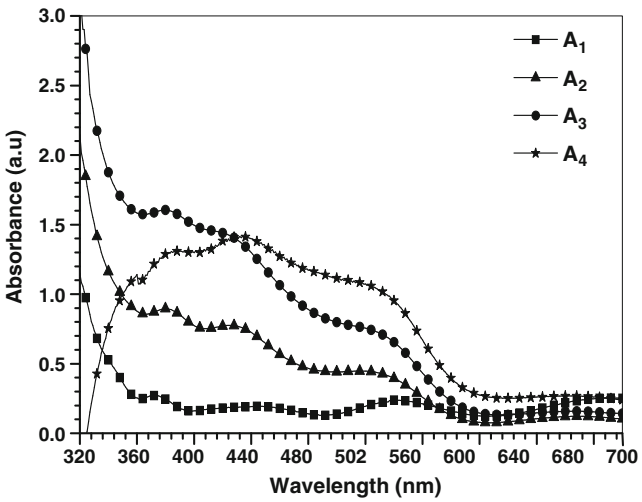

Fig. 3 UV-visible absorption spectra for pure Fe–TiO_2 sample A_1 and bilayered Fe–TiO_2/Zn–Fe_2O_3 samples A_2, A_3 and A_4 with varying upper layer thickness of Zn–Fe_2O_3 as 0.24, 0.48 and 0.72 μm, respectively

absorption spectra also indicate a very interesting case of the double bandgap state with a two-shoulder optical absorption slope, one typical of Fe–TiO_2, another one typical of Zn–Fe_2O_3.

Mott–Schottky plots were performed in the dark to investigate the nature of charge carriers in the semiconductor material and position of the bands in contact with the electrolyte during reaction. Mott–Schottky plots obtained for all the samples showed straight-line behaviour only in the region of monotonic part of the capacitance curve, this straight line gives apparent value of the flatband potential (V_{FB}). The flatband potential (V_{FB}) is an important factor in deciding the performance of material at metal oxide/electrolyte junction and was estimated for all samples using Mott–Schottky curves (Fig. 4). Positive slope of Mott–Schottky curves indicates the n-type semiconducting nature of the thin films. Calculated value of the flatband potential for all the samples have been given in Table 2. It can be seen that flatband potential for pure Fe–TiO_2 is approximately −0.59 V/SCE, which was observed to be

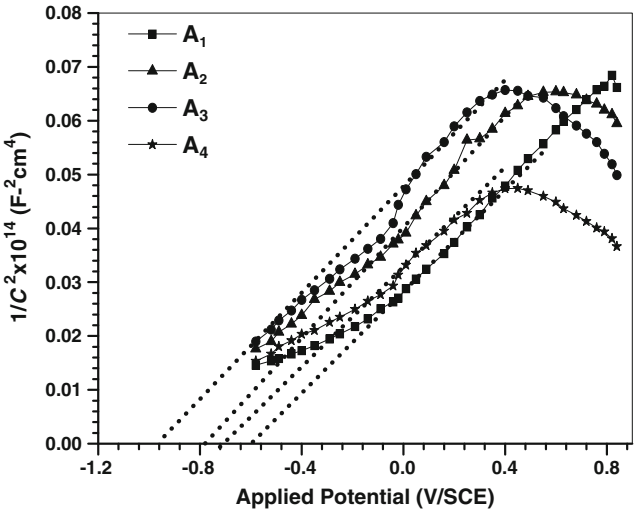

Fig. 4 Mott–Schottky curves for pure Fe–TiO_2 sample A_1 and bilayered Fe–TiO_2/Zn–Fe_2O_3 samples A_2, A_3 and A_4 with varying upper layer thickness of Zn–Fe_2O_3 as 0.24, 0.48 and 0.72 μm, respectively

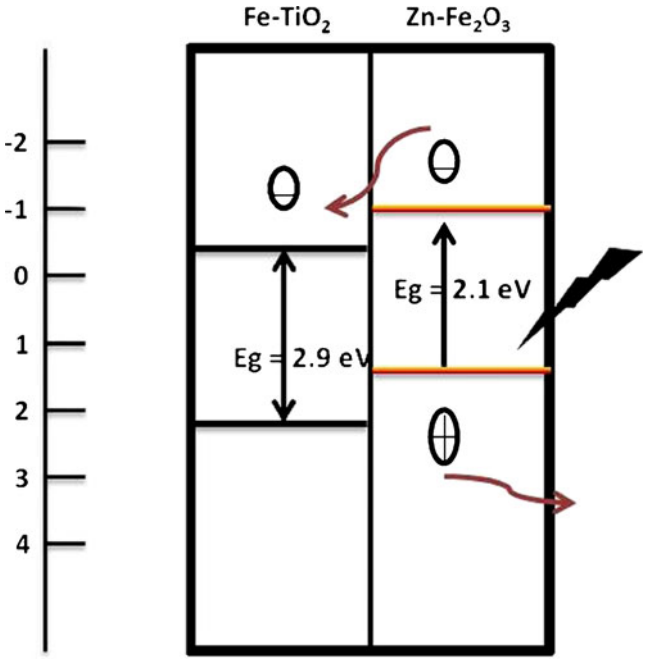

Fig. 5 Schematic energy band diagram for Fe–TiO_2/Zn–Fe_2O_3 thin film

larger for all the modified samples. Maximum value approximately −0.94 V/SCE was exhibited by the bilayered sample 'A_3', which has offered best photoelectrochemical response in this study. Negative shift in the flatband potential of pure Fe–TiO_2 with increasing Zn–Fe_2O_3 layer thickness is attributed to the Fermi level pinning by surface states in dark which further supports the enhanced photoelectrochemical response of the bilayered photoelectrode. It has been reported [19] that the negative shift in flatband potential is associated with (1) decrease in free energy for the transfer of charge from one metal oxide layer to the other and (2) increase in free energy for the charge recombination process. Therefore, such a situation will favour the photoelectrochemical response. The position of the conduction and the valence band edge of the pure Zn–Fe_2O_3 was calculated to be around −0.69 and 1.41 eV, respectively, from the flatband potential of pure Zn–Fe_2O_3 (−0.59 V/SCE) using the method reported by Schrebler et al. [20]. Similarly for the Fe–TiO_2, conduction and the valence band edge positions were calculated to be around −0.59 and 2.31 eV, respectively, using the method reported by Perera et al. [21]. On this basis, the dynamic flow of the photogenerated charge carriers across the interface of the bilayered Fe–TiO_2/Zn–Fe_2O_3 has been shown in Fig. 5 by locating the energy bands for pure Zn–Fe_2O_3 and Fe–TiO_2, respectively.

Photoelectrochemical behaviour of all the samples was studied by measuring the photocurrent density and open-circuit photovoltage. All the photoelectrodes were used in PEC cell for measurement of photocurrent density in 1 M NaOH under visible light illumination using 150 W Xenon lamp (Bentham). The photocurrent density was calculated by subtracting the dark current from current under illumination. It can be seen from Fig. 6 that modified photoelectrodes offered significantly better photoresponse in visible light than that of pure Fe–TiO_2 thin films. For modified photoelectrode 'A_3' with 480 nm thick upper layer of Zn–Fe_2O_3 photocurrent density was maximum at approximately 1,650 μA cm^{-2} at 0.95 V/SCE, which is almost nine times better than that of pure sample under visible light illumination (Table 2). This value of the photocurrent density is significantly better than the values reported by Yin et al. and Kuang et al. using the

Table 2 Photoelectrochemical performance of pure Fe–TiO_2 and bilayered Fe–TiO_2/Zn–Fe_2O_3 photoelectrodes

Sample identification	Resistivity (× 10^6 Ω cm)	Open-circuit photovoltage V_{oc},(V/SCE)	Photocurrent density at 0.95 V/SCE (μA cm^{-2})	Solar-to-hydrogen conversion efficiency (η%)	Flatband potential, V_{fb} (V/SCE)
A_1	6.5	0.29	262	0.10	−0.59
A_2	3.2	0.36	1423	0.61	−0.78
A_3	1.8	0.42	1650	0.77	−0.94
A_4	4.0	0.37	346	0.15	−0.70

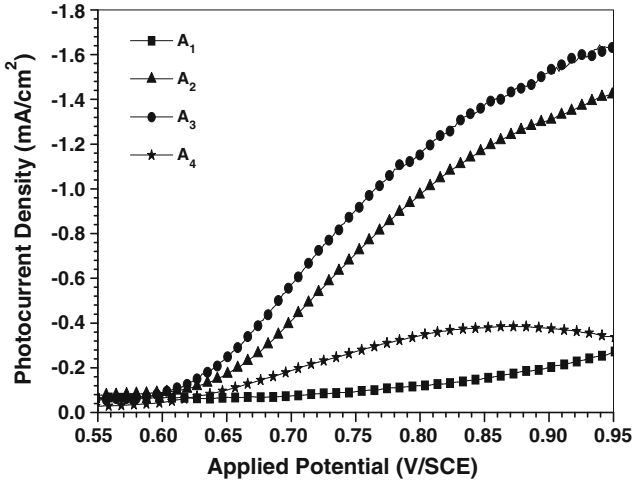

Fig. 6 Photocurrent density vs. applied potential curve for pure Fe–TiO_2 sample A_1 and bilayered Fe–TiO_2/Zn–Fe_2O_3 samples A_2, A_3 and A_4 with varying upper layer thickness of Zn–Fe_2O_3 as 0.24, 0.48 and 0.72 μm, respectively, under visible light illumination in 1 M NaOH electrolytic solution using 150 W visible light source of irradiance 150 mW cm^{-2} at the position of sample

layered structure of the TiO_2 [7, 22]. It was also observed that further increase in the thickness of Zn–Fe_2O_3 for sample 'A_4' exhibited a decrease in the photocurrent density. Thus, a perfect control over thickness is necessary to achieve higher photocurrent density.

The higher photoresponse of bilayered photoelectrode may be attributed to the favourable electron transfer at the interface of two materials, as the conduction band edge of Zn–Fe_2O_3 is higher than that of Fe–TiO_2. Under visible light irradiation, only Zn–Fe_2O_3 gets activated and electron–hole pairs are generated at the Zn–Fe_2O_3/electrolyte interface as shown in Fig. 5. It is expected that electrons generated in the conduction band of Zn–Fe_2O_3 are transferred and accumulated at the lower-lying conduction band of Fe–TiO_2, while holes accumulate at the valence band of Zn–Fe_2O_3. The photogenerated electron is then scavenged by the oxygen in water, and participates in the redox chemical reactions to split water and liberate hydrogen at counter electrode [7, 22]. Other factors contributing to enhanced photoresponse may be the extended absorption accompanied with significant red shift for the sample 'A_3', mixed oxide formation induced coupled effect between the energy bands of Fe–TiO_2 and Zn–Fe_2O_3, porous morphology for bilayered thin film sample permitting electrolyte to get in close proximity with the material [23].

To further elucidate the possible causes of marked increase in the visible light photoresponse of the bilayered samples, the resistivity of the samples were calculated as presented in Table 2. The resistivity was high for the pure Fe–TiO_2 thin film sample and decreased significantly for the bilayered samples favouring the flow of carriers within the bulk of the modified material. Also, the maximum value of flatband potential exhibited by sample 'A_3' supports maximum photocurrent density exhibited by this bilayered sample. However, decrease in photocurrent density exhibited by sample 'A_4' may be attributed to recombination of photogenerated electron/hole pair. An increased thickness of Zn–Fe_2O_3 increases the distance for the photogenerated carries to migrate to film surface, and thus enhance the recombination of the photogenerated carries [22]. Therefore, the optimum thickness of the Zn–Fe_2O_3 overlayered on Fe–TiO_2 obtained is 480 nm with respect to PEC response in this present work.

The solar-to-hydrogen conversion efficiency, (η%) was calculated for all the samples at 0.95 V/SCE using the equation given in [14] as:

$$\eta\% = [J_P(V_{rev} - V_{app})/I_o] \times 100 \quad (2)$$

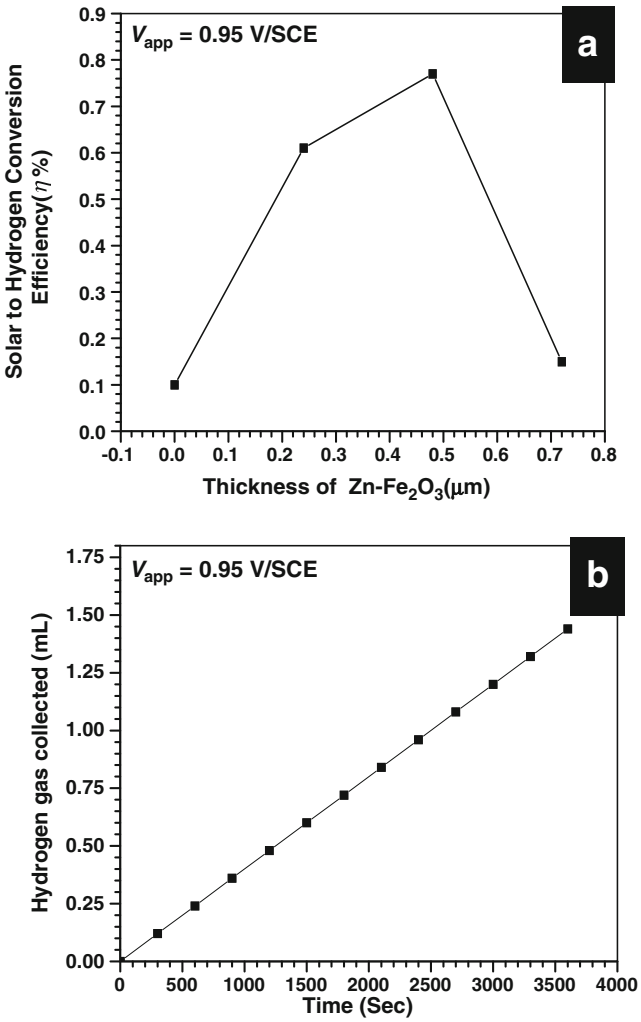

Fig. 7 (**a**) Solar-to-hydrogen conversion efficiency for all the samples at 0.95 V/SCE and (**b**) rate of hydrogen collection for the best performing photoelectrode A_3 using 150 W visible light source of irradiance 150 mW cm^{-2} at the position of sample

Where V_{rev} is the standard reversible potential, which is 1.23 V for water splitting reaction and V_{app} is the absolute value of applied potential at the photocathode that can be expressed as:

$$V_{app} = V_{meas} - V_{oc} \quad (3)$$

Where V_{meas} is the potential with respect to a reference electrode (e.g. SCE) at which photocurrent was measured, and V_{oc} is the electrode potential at open-circuit conditions (see Table 2) with respect to the same reference electrode and under the same illumination condition used for the photocurrent measurements. The solar-to-hydrogen conversion efficiencies with varying upper layer thickness of Zn–Fe_2O_3 has been shown in Fig. 7a. A maximum solar-to-hydrogen conversion efficiency of 0.77% was observed under visible light illumination for the modified photoelectrode 'A_3' offering the best visible light photoresponse. Hydrogen generated at Pt counter electrode was collected in an inverted test tube and measured by the water displacement method at 0.95 V/SCE (electrode potential, at which maximum STH was obtained) for the best photoresponsive bilayered sample. Measured rate of hydrogen production has been plotted in Fig. 7b showing maximum rate of production of hydrogen as 1.44 mL h^{-1} cm^{-2}. For the stability of the photoelectrode, experiment was run for multiple scans (15 times) and no change in the physical appearance of the sample was observed. Also, a linear plot obtained for amount of hydrogen generated with time (Fig. 7b) evidences the stability of the photoelectrode in electrolyte for water splitting reactions.

Conclusion

A bilayered photoelectrode obtained by depositing Zn–Fe_2O_3 layer on Fe–TiO_2 thin film exhibited significantly enhanced PEC response by extending absorption in visible light. Thickness of the overlayered Zn–Fe_2O_3 was found to be crucial in deciding structural, optical and photoelectrochemical properties of Fe–TiO_2. Maximum photocurrent density of 1,650 μA cm^{-2} at 0.95 V/SCE was exhibited by the bilayered sample Fe–TiO_2/Zn–Fe_2O_3, having 480 nm thick film of Zn–Fe_2O_3 over Fe–TiO_2. Improved absorption, mixed oxide formation and maximum value of flatband potential are responsible for better performance of this photoelectrode.

Acknowledgements We are thankful to the University Grant commission, New Delhi for partial financial support to carry out this work wide project no. 37-128/2009. The authors are also thankful to Dr. Dinesh Deva of DST Unit of Nanosciences, IIT Kanpur for the help in obtaining the XRD and AFM. We acknowledge the useful remarks of reviewers.

References

1. Chi CF, Liau SL, Lee YL (2010) The heat annealing effect on the performance of CdS/CdSe-sensitized TiO_2 photoelectrodes in photochemical hydrogen generation. Nanotechnology 21:025202–025208
2. Khan SUM, Shahry MA, Ingler WB (2002) Efficient photochemical water splitting by a chemically modified n-TiO_2. Science 27:2243–2245
3. Li H, Liu G, Chen S, Liu Q (2010) Novel Fe doped mesoporous TiO_2 microspheres: ultrasonic–hydrothermal synthesis, characterization, and photocatalytic properties. Physica E: Low-dimensional Systems and Nanostructures 42:1844–1849
4. Lei J, Li X, Li W, Sun F, Lu D, Yi J (2011) Arrayed porous iron-doped TiO_2 as photoelectrocatalyst with controllable pore size. Int J Hydrogen Energ 36:8167–8172
5. Tang X, Li D (2008) Sulfur-doped highly ordered TiO_2 nanotubular arrays with visible light response. J Phys Chem C 112:5405–5409
6. Ozaki H, Iwamoto S, Inoue M (2007) Improved visible–light responsive photocatalytic activity of N and Si co-doped titanias. J Mater Sci 42:4009–4017
7. Kuang SY, Yang LX, Luo SL, Cai QY (2009) Fabrication, characterization and photoelectrochemical properties of Fe_2O_3 modified TiO_2 nanotube arrays. App Surf Sci 255:7385–7388
8. Chen S, Paulose M, Ruan CM, Mor GK, Varghese OK, Kouzoudis D, Grimes CA (2006) Electrochemically synthesized CdS nanoparticle-modified TiO_2 nanotube-array photoelectrodes: preparation, characterization and application to photoelectrochemical cells. J Photochem Photobiol Chem 177:177–184
9. Tsuchiya H, Macak JM, Ghicov A, Taveira L, Schmuki P (2005) Self-organized porous TiO_2 and ZrO_2 produced by anodization. Corrosion Sci 47:3324–3335
10. Wang J, Han Y, Feng M, Chen J, Li X, Zhang S (2011) Preparation and photoelectrochemical characterization of WO_3/TiO_2 nanotube array electrode. J Mater Sci 46:416–421
11. Rincon ME, Trujillo ME, Avalos J, Casillas N (2007) Photoelectrochemical process at interfaces of nanostructured TiO_2/carbon black composites studied by scanning photoelectrochemical microscopy. J Solid State Electrochem 11:1287–1294
12. Liu H, Gao L, Mizutani M (2005) Preparation and properties of nanocrystalline α-Fe_2O_3 sensitized TiO_2 nanosheets as a visible light photocatalyst. J Am Ceram Soc 89:370–373
13. Sharma P, Kumar P, Deva D, Shrivastav R, Dass S, Satsangi VR (2010) Nanostructured Zn-Fe_2O_3 thin film modified by Fe-TiO_2 for photoelectrochemical generation of hydrogen. Int J Hydrogen Energ 35:10883–10889
14. Kumari S, Tripathi C, Singh AP, Chauhan D, Shrivastav R, Dass S, Satsangi VR (2006) Characterization of Zn-doped hematite thin films for photoelectrochemical splitting of water. Curr Sci 91:1062–1064
15. Kumari S, Singh AP, Sonal DD, Shrivastav R, Dass S, Satsangi VR (2010) Spray pyrolytically deposited nanoporous Ti^{4+} doped hematite thin films for efficient photoelectrochemical splitting of water. Int J Hydrogen Energ 35:3985–3990
16. Shannon RD (1976) Revised effective ionic radii and systematic studies of interatomic distances in halides and chalcogenides. Acta Crystallogr A32:751–767
17. Amorelli A, Evans JC, Rowlands CC (1989) Electron paramagnetic resonance study of transition metal ion impregnated brookite titanium dioxide powders. J Chem Soc Faraday Trans 85:4031–4038
18. Thimsen E, Biswas S, Lo CS, Biswas P (2009) Predicting the band structure of mixed transition metal oxides: theory and experiment. J Phys Chem C 113:2014–2021
19. Bandara J, Pradeep UW (2006) Variation of flatband potential of oxide nanocrystalline particles with core-shell structured semiconductor-MgO composites. Sri Lanka J Phy 7:23–28

20. Schrebler R, Llewelyn C, Vera F, Cury P, Munoz E, Río R, Meier HG, Córdova R, Dalchiele EA (2007) An electrochemical deposition route for obtaining α-Fe_2O_3 thin films II. EQCM study and semiconductor properties. Electrochem Solid State Lett 10:D95–D99
21. Perera VPS, Jayaweera PVV, Pitigala PKDDP, Bandaranayake PKM, Hastings G, Perera AGU, Tennakone K (2004) Construction of a photovoltaic device by deposition of thin films of the conducting polymer polythiocyanogen. Synthetic Metals 143:283–287
22. Yin J, Bie LJ, Yuan ZH (2007) Photoelectrochemical property of $ZnFe_2O_4/TiO_2$ double-layered films. Mat Res Bull 42:1402–1406
23. Harris CJ, Belcher WJ, Dastoor PC (2007) Effect of film thickness and morphology on the performance of photoelectrochemical cells based on poly(terthiophene). Sol Energ Mater Sol Cell 91:1127–1136